Biochimica et Biophysica Acta 1847 (2015) 223–230

Contents lists available at ScienceDirect

Biochimica et Biophysica Acta

journal homepage: www.elsevier.com/locate/bbabio

The rate of second electron transfer to Q_B^- in bacterial reaction center of impaired proton delivery shows hydrogen-isotope effect

Ágnes Maróti [a], Colin A. Wraight [b,c,1], Péter Maróti [d,*]

[a] Department of Pediatrics, University of Szeged, Hungary
[b] Center for Biophysics and Computational Biology, University of Illinois, Urbana, IL 61801-3838, USA
[c] Department of Plant Biology, University of Illinois, Urbana, IL 61801-3838, USA
[d] Department of Medical Physics, University of Szeged, Hungary

ARTICLE INFO

Article history:
Received 2 September 2014
Received in revised form 31 October 2014
Accepted 5 November 2014
Available online 13 November 2014

Keywords:
Bacterial photosynthesis
Reaction center protein
Flash-induced proton delivery
Protonation mutant
Solvent isotope effect

ABSTRACT

The 2nd electron transfer in reaction center of photosynthetic bacterium *Rhodobacter sphaeroides* is a two step process in which protonation of Q_B^- precedes interquinone electron transfer. The thermal activation and pH dependence of the overall rate constants of different RC variants were measured and compared in solvents of water (H_2O) and heavy water (D_2O). The electron transfer variants where the electron transfer is rate limiting (wild type and M17DN, L210DN and H173EQ mutants) do not show solvent isotope effect and the significant decrease of the rate constant of the second electron transfer in these mutants is due to lowering the operational pK_a of Q_B^-/Q_BH: 4.5 (native), 3.9 (L210DN), 3.7 (M17DN) and 3.1 (H173EQ) at pH 7. On the other hand, the proton transfer variants where the proton transfer is rate limiting demonstrate solvent isotope effect of pH-independent moderate magnitude (2.11 ± 0.26 (WT + Ni^{2+}), 2.16 ± 0.35 (WT + Cd^{2+}) and 2.34 ± 0.44 (L210DN/M17DN)) or pH-dependent large magnitude (5.7 at pH 4 (L213DN)). Upon deuteration, the free energy and the enthalpy of activation increase in all proton transfer variants by about 1 kcal/mol and the entropy of activation becomes negligible in L210DN/M17DN mutant. The results are interpreted as manifestation of equilibrium and kinetic solvent isotope effects and the structural, energetic and kinetic possibility of alternate proton delivery pathways are discussed.

1. Introduction

Proton transfer reactions (acid-base catalysis in enzyme activity [1] or transport of protons over large distances in bioenergetics [2]) are of crucial significance in biology [3]. They need well defined atomic structure (gramicidin [4] and carbonic anhydrase [5]), substantial energetic constraints (aquaporin [6]) and, in many cases, are coupled to conformation changes (bacteriorhodopsin [7]) or electron transfer [8] (cytochrome oxidase [9] and oxygen evolution [10] and quinone reduction cycle of photosynthesis [11]) in the protein. In photosynthetic reaction center (RC) from purple bacteria, the proton coupled electron transfer is evoked by two subsequent saturating flashes and results in full reduction of quinone (Q) at the secondary quinone binding site Q_B: $Q + 2e^- + 2H^+ \rightarrow QH_2$ [12]. The same proton path, formed by acidic cluster around Q_B is used to deliver protons both on the first and on the second electron transfers (Fig. 1, [13,14]). The nature of the proton accepting group(s), however, is quite different. On the first flash, the protons are accepted by an array of ionizable residues in the cluster as their pK_a values increase in response to the Q_B^- formation [15–17]. On the second flash, the proton is trapped at any pH by Q_B^- itself. The rate of the $Q_A^-Q_B^- + H^+ \rightarrow Q_AQ_BH^-$ second electron transfer depends on the free energy gap $\Delta G_{AB}^{(2)}$, as has been shown by driving force assay using RC preparations with Q_A replaced by low-potential quinones [18]. This finding has been interpreted as an evidence of a fast, non-rate-limiting protonation of a semiquinone anion ($Q_B^- + H^+ \rightarrow Q_BH$) followed by a rate-limiting nonadiabatic ET reaction ($Q_BH \rightarrow Q_BH^-$) with rate constant $k_{et}^{(2)}$ (Fig. 2, [13,18]). Thus, the 2nd electron transfer proceeds with an observed rate of

$$k_{AB}^{(2)} = k_{et}^{(2)} \cdot f(Q_BH), \quad (1)$$

where $f(Q_BH)$ is the fraction of the semiquinone in the protonated state.

In contrast to the first electron transfer, there is no conformational control on the second electron transfer. It is not surprising, because both Q_B^- and the ubiquinol-anion Q_BH^- are likely to be fixed in similar positions [19]. However, the contribution of the protonic relaxation to the kinetics of the 2nd electron transfer is an open question. Due to the low pK_a value of the Q_B^-/Q_BH couple, the absence of a notable protonic relaxation can be expected in wild type and in mutants where

Abbreviations: ET, electron transfer; PT, proton transfer; P, bacteriochlorophyll dimer; Q_A and Q_B, primary and secondary quinone acceptors, respectively; RC, (bacterial) reaction center

* Corresponding author at: Department of Medical Physics, University of Szeged, Rerrich Béla tér 1, Szeged, H-6720 Hungary. Tel.: +36 62 544 120; fax: +36 62 544 121.
E-mail address: pmaroti@sol.cc.u-szeged.hu (P. Maróti).

[1] Passed away on 10 July 2014. This work is dedicated to his memory.

http://dx.doi.org/10.1016/j.bbabio.2014.11.002
0005-2728/

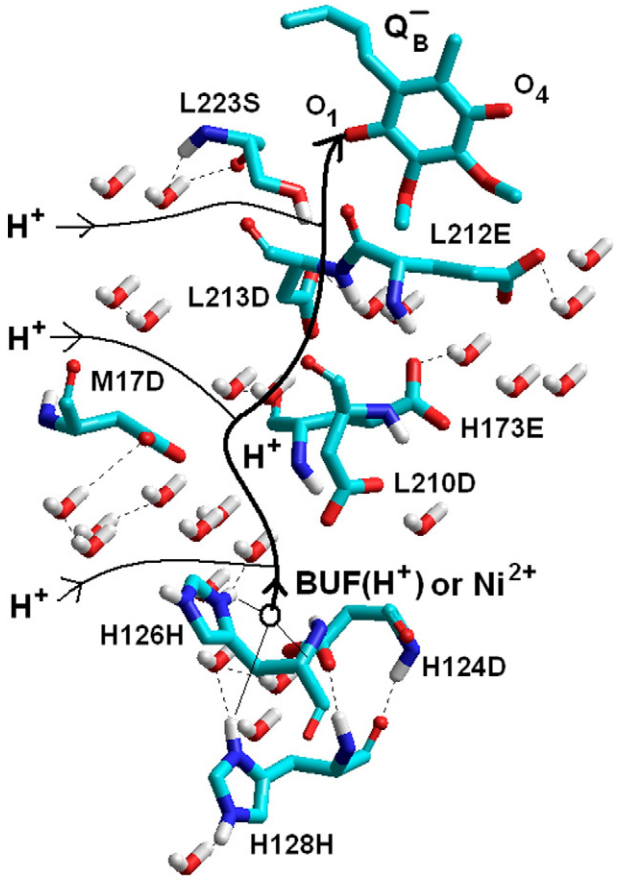

Fig. 1. Key protonatable amino acids and water molecules of the proton delivery pathway from the proton entry point BUF(H^+) to Q_B^- semiquinone after the second flash in native RC of *R. sphaeroides*. The proton transport is severely impaired by ligation of divalent transition metal ions (e.g. Ni^{2+}) to the H126H/H128H/H124D cluster or by replacement of the protonatable amino acids to nonprotonatable residues by single (or double) mutations. The alternative (by-pass) proton pathways are connected to the main pathway above the deletion sites.
The structure was taken from Brookhaven Protein Databank 3I4D (www.rcsb.org).

the electron transfer is the rate limiting step. On the other hand, in mutants of PT limitation, the rate becomes independent of $\Delta G_{AB}^{(2)}$ [20] and thereby the proton relaxation control over the second electron transfer might be imposed.

The recognition of protonic relaxation modes could be facilitated by the notion that the protonic component should depend on the H/D isotope substitution as shown below by two examples: 1) The slow (1–30 μs) phase of the reduction of the photo-oxidized primary donor of the photosystem II ($P680^+$) by a redox-active tyrosine Y_Z is sensitive to the H/D substitution and has been attributed to the protonic relaxation [21]. 2) The two hydrogen-bonded protons associated with Q_A of reaction centers from *Rhodobacter sphaeroides* can be exchanged with deuterons from solvent D_2O. The rate of $P^+Q_A^- \rightarrow PQ_A$ electron-transfer, k_{PA} was found to increase slightly with deuterium exchange up to a maximum $k_{PA}(D^+)/k_{PA}(H^+) = 1.06$ [22]. The solvent isotope effect indicates that these protons play a role in the vibronic coupling associated with electron transfer of charge recombination.

These examples indicate that there seems to be great potential in H/D exchange experiments while light-induced proton binding/unbinding is taking place in bacterial RC. Incubation in D_2O caused pH (pD)-dependent slowing of the H^+/D^+ binding rate after the first flash [23]. A maximum isotope effect of the apparent proton binding rate constant $k_{on}(H)/k_{on}(D) = 3.0$ was found. It is worth to carry out similar isotope measurements with the 2nd ET of various proton transfer RC variants. These RCs impede the normal fast function of the bucket brigade mechanism of PT at well defined locations: native RC treated with divalent metal ions at the proton entry point [24,25], L210DN/M17DN double mutation between L210D and M17D [26,27] and L213DN single mutation at L213 close (<5 Å) to Q_B [20,28]. The proton delivery with significantly increased free energy of activation will be the bottle neck of the observed 2nd ET (Fig. 2). The proton equilibrium partitioning (see Eq. (1)), and therefore the fraction of protonated sites of Q_B^- may be affected by H/D exchange (equilibrium isotope effect). Additionally, if proton pathways are limited by bond-breaking steps, the observed rate will be sensitive to deuteration of the RC (kinetic isotope effect). These effects can be used to elucidate the PT mechanisms including rate limiting steps, transition states and alternate pathways.

2. Materials and methods

2.1. Reagents and reaction centers

Ethanolic solutions of ferrocene, ethyl ferrocene and DAD (diaminodurene) were prepared fresh prior use. Cytochrome-*c* (horse heart grade VI) was reduced (>95%) by hydrogen gas on platinum black and filtered (0.2 μm pore size acetate filter). Experiments were carried out in mixture (2–2 mM) of buffers (citric acid, Mes, Mops, Pipes, Tris, Ches and Caps) whose pK_a values are close to the pH value of the solution.

Details of the molecular biological techniques in generating *Rhodobacter (R.) sphaeroides* with mutant RCs have been described earlier [28]. Reaction centers from *R. sphaeroides*, strain R-26, wild type and mutants were isolated in LDAO (lauryldimethylamine *N*-oxide) as described earlier [29]. The RC was concentrated to ~100 μM by centrifugation (Amicon Centricon-30) and dialyzed 1–2 days at 4 °C against 1 mM Tris buffer (pH 8.0) and 0.03% Triton X-l00 detergent before use. As RCs isolated this way showed little secondary quinone activity, it was reconstituted by addition of ubiquinone-10 solubilized in ethanol in large excess ([UQ]/[RC] >10) to RC prior to use.

2.2. Electron transfer measurements

Kinetics of flash-induced ET was measured by absorption changes using a single beam spectrophotometer of local design [29]. The rates of charge recombination ($P^+Q_B^- \rightarrow PQ_B$) were obtained by monitoring the recovery of the dimer (P) absorbance at 430 nm, following a saturating exciting flash. The concentration of RCs was determined using an extinction coefficient of 26 $mM^{-1}\,cm^{-1}$. The occupancy of the Q_B site (typically ~90% at pH 8.0) was determined from the relative amplitudes of the slow and fast kinetic phases of charge recombination [30].

The rate constants of the second ET to Q_B^- were determined by monitoring the decay of absorbance of the semiquinones (Q_A^- and Q_B^-) at wavelength 450 nm following a second saturating flash in RC solution containing an exogenous reductant to reduce the oxidized dimer P^+. Depending on the magnitude of $k^{(2)}{}_{AB}$, different donors were applied to reduce P^+: mammalian cytochrome *c* or cytochrome c_2 (fast donation) and ferrocene (slow donation at low (2–10 μM) concentrations and fast donation at high (400 μM) concentration) [31]. With the use of different donors, their disadvantages were tried to minimize. A small fraction of cytochrome c^{2+} under our conditions did follow a relatively slow photo-oxidation (in the range of several hundreds of microseconds) after the second flash, and it could have kinetic contribution to the observed absorption change at 450 nm. To avoid the overlap in the (sub) millisecond range, ferrocene, a much slower donor than the cytochrome c^{2+} was also applied. Although the redox changes of ferrocene do not have contribution in this optical range, the observed kinetics includes the large absorption change from P/P^+ and its separation from that of Q/Q^- needs careful multiexponential peeling of the traces carried out by Marquardt's least square method.

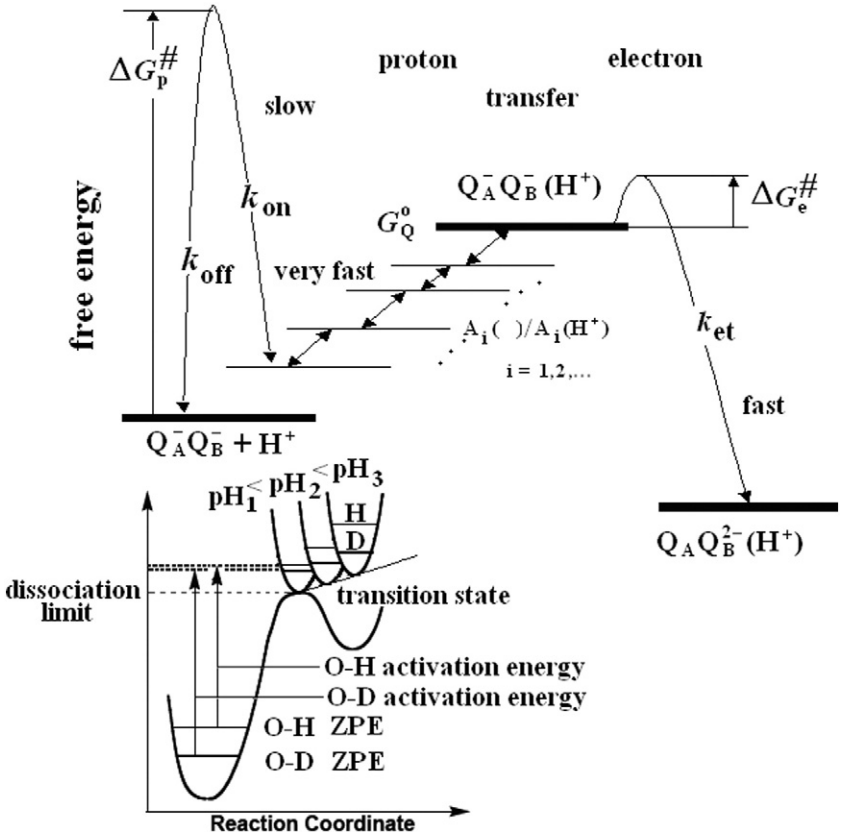

Fig. 2. Proton coupled second ET in bacterial RC. The fast interquinone ET (k_{et}) is preceded by faster (WT) or slower (PT variants) proton equilibration with Q_B^-. The rate limiting step of proton delivery to Q_B^- is attributed to enhanced proton free energy of activation ($\Delta G_p^{\#}$) with k_{on} and k_{off} forward and back PT rate constants, respectively. Depending on mutations and ways of impedance in the proton pathway, the bottle neck can occur in different locations (amino acids, A_i) of the proton delivery network. Kinetic solvent isotope effect is attributed to difference of the zero point energies in the reactant and transition states that can show pH-dependence. Notations: G^o_Q — standard free energy level of semiquinone at Q_B, A_i — intermediate protonatable residue (amino acid or water) in the chain and ZPE — zero point energy of O – H(D) vibration.

The PT mutants (e.g. L213DN) can trap Q_B^- very effectively and the relaxation to the PQ_AQ_B state is very long [20,28]. Therefore, most measurements were performed with a fresh sample for each measurements.

2.3. Hydrogen isotope measurements

The rate constants of $k^{(2)}_{AB}$ are sensitive to measurement conditions (RC preparation, pH, detergent concentration, etc.) and their standard deviation can be commeasurable to the isotope effect, i.e. the difference between rates measured in water and heavy water. Instead of comparative measurements on two separately prepared samples, the RCs from a highly concentrated stock (>300 μM) in H_2O (or D_2O) were diluted into D_2O (or H_2O) gradually while the salt and detergent concentrations were held constant. The observed rates were plotted as a function of dilution and a linear fit to the measured rates offered $k^{(2)}_{AB}(D)$ and $k^{(2)}_{AB}(H)$ as interception at heavy water ($[D_2O] / ([D_2O] + [H_2O]) = 1$) and normal water ($[D_2O] / ([D_2O] + [H_2O]) = 0$), respectively. The isotope effect is characterized by the negative slope of the straight line, i.e. $k^{(2)}_{AB}(H)/k^{(2)}_{AB}(D)$.

All pH(D) measurements were made with a glass electrode (Radiometer, Copenhagen, Denmark) and were reported in D_2O as pD = apparent pH + 0.40, to indicate the corrected D^+-ion concentration for the glass electrode solvent isotope artifact [32,33]. The "apparent pH" means the actual pH meter reading. Deuterated acid (DCl) and base (NaOD) were used for pD adjustment. The glass electrode had been standardized with conventional buffer mixtures (in H_2O) at pH 7.0 and 11.0 (alkaline range) or 4.0 (acidic range).

3. Results

3.1. Rate constant of second electron transfer, $k^{(2)}_{AB}$ and operational pK_a of Q_B^-/Q_BH

The proton-coupled ET rate constant $k^{(2)}_{AB}$ ($Q_A^-Q_B^- + H^+ \rightarrow Q_AQ_BH^-$) was measured by monitoring the absorption changes at 450 nm due to the simultaneous disappearance of two semiquinones (Q_A^- and Q_B^-) after the second saturating flash in the presence of an exogenous donor. The donor was selected to make the electron donation to the RC either faster (cytochrome c^{2+}) or slower (various ferrocene compounds at low concentrations) than the second ET because of kinetic separation of the second ET from P^+ donation (cyt c^{2+} $P^+ \rightarrow$ cyt c^{3+}P) and/or elimination of the charge recombination ($P^+Q_A^-Q_B^- \rightarrow PQ_AQ_B^-$). The rate constant $k^{(2)}_{AB}$ measured in native RC was not dramatically affected in L210DN, M17DN and H173EQ electron transfer mutants (Fig. 3a). The decrease from the native value was small (about 3-fold) in L210DN and M17DN mutants but significantly larger (about 200-fold) in H173EQ mutant. In contrast, the PT mutants (L213DN single mutant and L210DN/M17DN double mutant together with native RC poisoned by transient divalent ions) show much larger (up to 4 orders of magnitude) decrease relative to that of the native value (Fig. 3b) in nice agreement with earlier measurements [20,26].

The pH profiles of $k^{(2)}_{AB}$ of electron and proton transfer limited RCs show marked differences. The logarithms of $k^{(2)}_{AB}$ of PT variants display (with good approximation) linear pH dependence throughout the entire pH range from 4 to 9. The electron transfer RC mutants, however, describe monotonously decreasing function with gradually increasing slope: it is

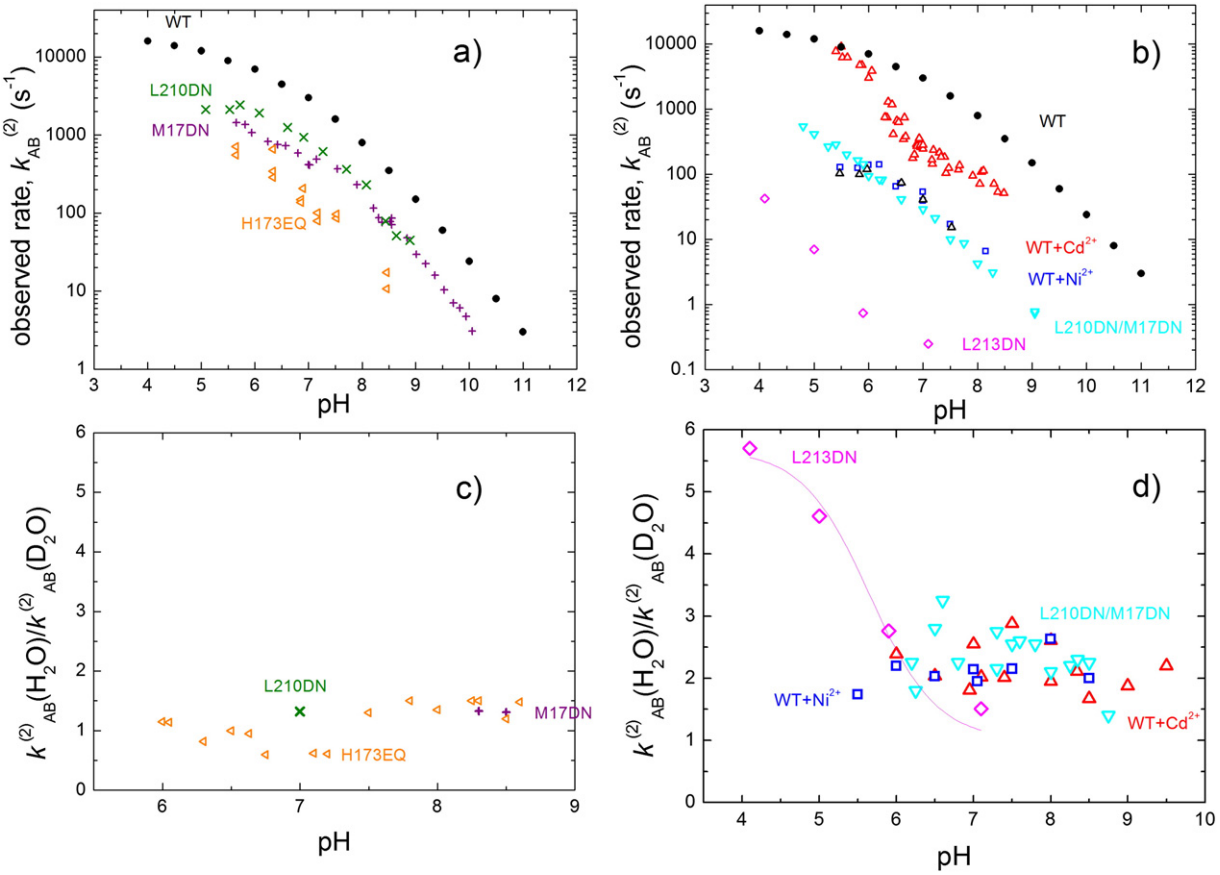

Fig. 3. pH dependence of the observed rate constants ($k^{(2)}_{AB}$, panels a and b) and solvent isotope effect ($k^{(2)}_{AB}(H)/k^{(2)}_{AB}(D)$, panels c and d) of second ET for various RC strains of ET (panels a and c) and PT (panels b and d) limitation. The pH-dependence of the isotope effect in the L213DN mutant is approximated by a Henderson–Hasselbalch function with amplitude of 5.7 and pK_a = 5.65 (panel d). Symbols: ● (WT), □ (WT + Ni^{2+}), △ (WT + Cd^{2+}), ◊ (L213DN), × (L210DN), + (M17DN), ◁ (H173EQ) and ▽ (L210DN/M17DN). Conditions: 1.0–4.0 μM RC, 0.02% Triton X-100, 40 μM UQ_{10}, 5 mM KCl, T = 293 K, 2–2 mM buffer mix, 20 μM cyt c^{2+} or 2–8 μM/300–500 μM (ethyl-, methyl)ferrocene (depending on $k^{(2)}_{AB}$, see Materials and methods) and 100 μM $CdCl_2$ or 1 mM $NiCl_2$ in metal treated WT RC.

small in the acidic pH range, becomes more pronounced in the neutral and slightly alkaline pH regions and approaches the limiting value of −1 in the highly alkaline pH range. The measured rates are pH-dependent because the population of Q_BH is pH dependent. In native (and other ET mutant) RCs, the rate limiting ET is preceded by very fast proton equilibrium $Q_A^-Q_B^- + H^+ \leftrightarrow Q_A^- Q_BH$. In the simplest case, the protonated fraction, $f(Q_BH)$ follows the Henderson–Hasselbalch equation, but the complex electrostatics of the protein interior results in an extended pH-dependence [17] that can be formally approximated by a Henderson–Hasselbalch function with pH-dependent (operational) pK_a values:

$$f(Q_BH) = \frac{10^{pK_a(pH)-pH}}{1+10^{pK_a(pH)-pH}} \quad (2)$$

By inserting Eq. (2) into Eq. (1) and taking $k^{(2)}_{et} = 1 \cdot 10^6\ s^{-1}$ [34], the pH-dependence of the operational pK_a of Q_BH can be derived from the measured $k^{(2)}_{AB}$ values in wild type and some other ET mutant RCs (Fig. 4). At pH 7, the operational pK_a values of the native semiubiquinone-10 are 4.5 (WT) [34–36], 3.9 (L210DN), 3.7 (M17DN) and 3.1 (H173EQ) which are in good accordance with values obtained from temperature dependence of the second ET [37]. In absence of any electrostatic interactions between RC and Q_B^-, one would expect a constant pK_a value throughout the pH scale. This is clearly not the case. In the acidic pH range, the increase of the operational pK_a is steep (close to 1) and levels off in the alkaline pH region.

3.2. Solvent isotope effect of $k^{(2)}_{AB}$

The solvent isotope effect was studied by comparison of $k^{(2)}_{AB}$ measured in water (H_2O) and in heavy water (D_2O) under otherwise identical conditions. The proton → deuterium exchange in the protein was initiated at t = 0 by injecting the concentrated stock of RC into

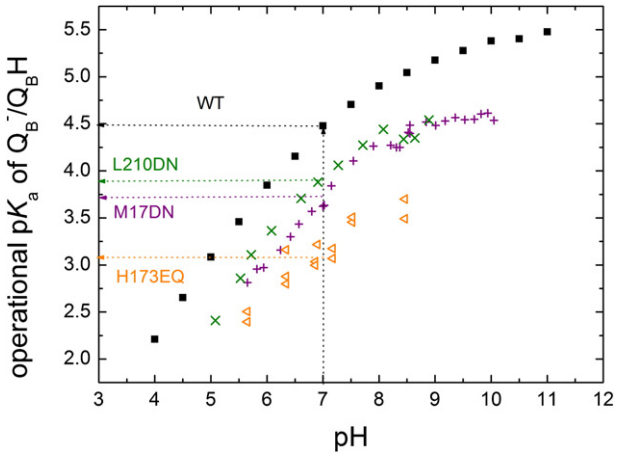

Fig. 4. pH-dependence of the operational pK_a values of Q_B^-/Q_BH calculated from the rate constants of the second ET limited by ET (Fig. 3a) according to Eqs. (1) and (2). The rate constant of intrinsic ET was taken $k^{(2)}_{et} = 1 \cdot 10^6\ s^{-1}$ [34]. The operational pK_a values for some ET mutants at pH 7 are indicated by arrows.

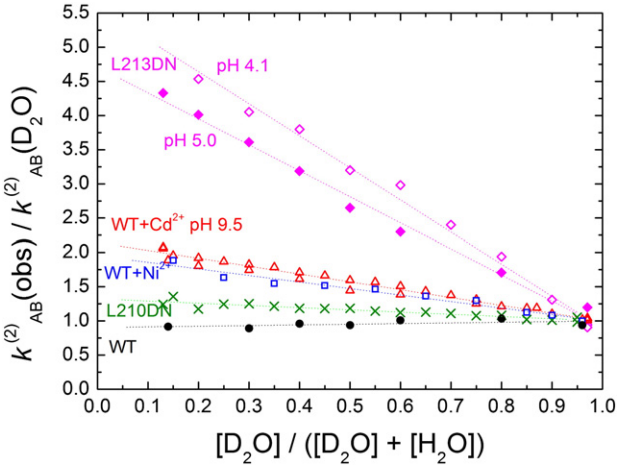

Fig 5. Solvent isotope effect of $k^{(2)}_{AB}$ of WT RC (●), L210DN (×) and proton transfer variants WT+Ni^{2+} (□), WT+Cd^{2+} (Δ) and L213DN (◊, pH 4.1 and ◆, pH 5.0) in mixture of water (H_2O) and heavy water (D_2O). Proton ↔ deuterium exchange was carried out by repeated dilution of the RC stock solutions in H_2O or D_2O by D_2O or H_2O, respectively.

D_2O (Fig. 5). The isotope shift due to deuteration of the protonatable groups in the proton delivery pathway occurred "promptly" (i.e., within 2 h [23]) and no further changes in the rate of the second ET were observed after prolonged (24 h) incubation in D_2O. The reaction mixture was split into two equal parts and they were diluted repeatedly by D_2O and H_2O, respectively. The concentration of the ingredients (detergent, salt and buffers) remained unchanged during the dilution. The D_2O content of the sample could change between >95% and ~10% at the beginning and at the end of the dilution, respectively. The dilution carried out in the reverse direction offered similar results: the observed $k^{(2)}_{AB}$ decreased in a linear manner with increase of the D_2O content of the solvent. The intersections of the best fit straight line to the data at 0% D_2O (H) and 100% D_2O (D) deliver $k^{(2)}_{AB}$(H) and $k^{(2)}_{AB}$(D) and their ratio measures directly the solvent isotope effect.

As expected, there is no solvent isotope effect in native RC (Fig. 5) and the ET mutants show also negligible isotope effect, e.g. 1.11 ± 0.33 for the H173EQ mutant (Fig. 3c). In contrast to the wild type and ET mutants, the PT variants demonstrate marked but moderately large solvent isotope effects (Fig. 3d): 2.11 ± 0.26 (WT + Ni^{2+}), 2.16 ± 0.35 (WT + Cd^{2+}) and 2.34 ± 0.44 (L210DN/M17DN double mutant) and do not depend on pH. The L213DN mutant shows unique features: in the strongly acidic pH range (pH ≈ 4), the solvent isotope effect is large (≈6) which drops progressively upon increase of the pH to a low (≈1.4) value that approaches the isotope effect of proton/deuterium diffusion in aqueous solution.

3.3. Temperature-dependence of $k^{(2)}_{AB}$ in proton transfer variants

The observed large change of the rate constant of the second ET in different RC variants can be attributed to change of the free energy of activation ($\Delta G^{\#}$). Lower rate corresponds to higher free energy change of activation and the correlation is logarithmic. According to the transition state theory (TST [38]),

$$k^{(2)}_{AB} = \frac{k_B T}{h} \exp\left(\frac{-\Delta G^{\#}}{RT}\right), \quad (3)$$

where T is the temperature, h denotes the Planck's constant and k_B and R are the Boltzmann factor and universal gas constant, respectively. (The transmission coefficient is taken 1.) The function of $\ln\left(\frac{k^2_{AB}\cdot h}{k_B T}\right)$ vs. $1/T$ should give a straight line of slope ($=-\Delta H^{\#}/R$) characteristic to the change of activation enthalpy, $\Delta H^{\#}$ and intersection ($=-\Delta S^{\#}/R$) characteristic to the change of activation entropy, $\Delta S^{\#}$ (Eyring plot). The observed activation parameters relate to the rate limiting step of $k^{(2)}_{AB}$. As the second ET is a combination of electron and proton transfer reactions, the observed activation may correspond to either electron or proton reactions. In PT mutants, the analysis is simplified as the measured change of activation free energy (enthalpy and entropy) relates to the bottle neck of the series of protonation steps in the proton delivery pathway.

Fig. 6 demonstrates the Eyring plot of the PT variant of the L210DN/M17DN double mutant in the physiological temperature range. The measured points fit to a straight line with $\Delta G^{\#}$ = 15.6 kcal/mol, $\Delta H^{\#}$ = 10.1 kcal/mol and $T \cdot \Delta S^{\#} = -5.52$ kcal/mol activation free energy, enthalpy and entropic energy, respectively, at room temperature and pH 7.5. As the PT is the rate limiting step of $k^{(2)}_{AB}$, one can expect effect of proton → deuterium exchange in the protein. Indeed, significant modification of the activation parameters is observed after deuteration of the sample. Somewhat less, but still considerable changes can be seen upon isotope (deuterium) exchange in other protonation RC variants investigated in this study: WT + Cd^{2+}, WT + Ni^{2+} and L213DN (Fig. 7). In all cases, the activation parameters of the free energy and enthalpy shift to larger values and the entropic contributions become smaller after deuteration. As expected, the WT RC has much less free energy and enthalpy of activation and shows no isotope effect.

4. Discussion

In native RC, the second interquinone ET occurs after very fast partial proton uptake by Q_B^-. In various PT variants used in this study the proton delivery to Q_B^- can be slowed down dramatically and will become the rate determining step of the ET. Under these conditions, the exchange of hydrogen to deuterium in solvent and RCs imposes reversible isotope effects of $k^{(2)}_{AB}$: upon dilution in H_2O and ultrafiltration of the RCs, the rate constant can be restored to a value typically measured in H_2O. The discussion will extend on the origin, magnitude and pH dependence of the observed isotope effect found in the various RC variants and will cover the structural and energetic aspects of the possible alternative proton delivery pathways to Q_B^-.

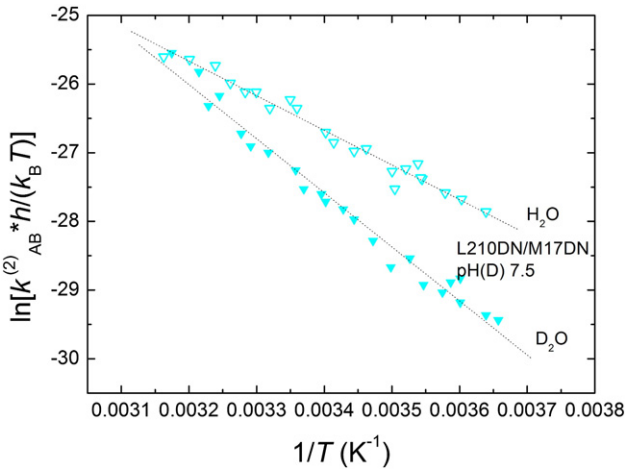

Fig. 6. Temperature dependence (Eyring plot) of the rate constants of the second ET ($k^{(2)}_{AB}$) in RC of double mutant L210DN/M17DN in water (H_2O, ▽) and heavy water (D_2O, ▼). Activation enthalpy change (slope): $\Delta H^{\#}$ = 10.1 kcal/mol (H_2O) and 15.6 kcal/mol (D_2O), activation entropy change (intersection): $T\cdot\Delta S^{\#}$ = –5.5 kcal/mol (H_2O) and −0.47 kcal/mol (D_2O) and activation free energy change: $\Delta G^{\#}$ = 15.6 kcal/mol (H_2O) and 16.1 kcal/mol (D_2O). Conditions: 1.0 μM RC, 0.02% Triton X-100, 40 μM UQ_{10}, 5 mM NaCl, 2.5 mM Mops, 2.5 mM Tris, pH(D) 7.50 and 300 μM ethyl ferrocene. Notations: h — Planck's constant and k_BT — Boltzmann term.

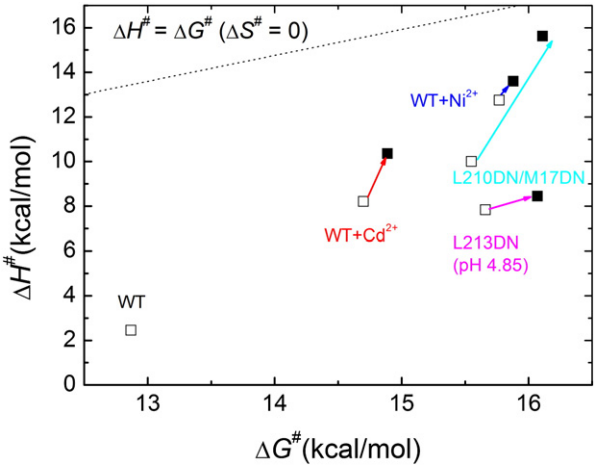

Fig. 7. Eyring (transition state theory) activation parameters ($\Delta H^{\#}$ vs. $\Delta G^{\#}$) of the second ET of RCs of PT variants (open symbols) and transitions due to deuteration (closed symbols). The states of no entropic changes are indicated by a straight line.

4.1. The origin of solvent isotope effect of $k^{(2)}_{AB}$ in RC

The observed rate of the second ET is the combination of the rates of protonation of the slowest step (the sum of binding and unbinding rates: $k_p = k_{on} + k_{off}$) and the interquinone ET, k_{et}. According to the reaction scheme in Fig. 2,

$$k^{(2)}_{AB} = \frac{k_{on} + k_{off} + k_{et} - \sqrt{(k_{on} + k_{off} + k_{et})^2 - 4 \cdot k_{on} \cdot k_{et}}}{2}. \quad (4)$$

In ET limit ($k_p \gg k_{et}$), we obtain $k^{(2)}_{AB} = k_{et}/(1 + k_{off}/k_{on})$ that is equivalent with Eq. (1). No isotope effect is expected unless k_{off}/k_{on} that relates to the proton dissociation constant of the semiquinone Q_B^- might show up equilibrium isotope effect. This effect, however, is negligible ($pK_D - pK_H < 0.1$), as very small if any isotope effect is observed in the ET mutants (Fig. 3c).

In PT limit ($k_p \ll k_{et}$), Eq. (4) offers $k^{(2)}_{AB} = k_{on}$ which means that the observed rate is determined by the rate constant of proton (deuterium) binding only. In this extreme case, $k^{(2)}_{AB}$ might be sensitive to changes due to deuteration (discussed below). In intermediate case, when the rates of protonation and ET are commeasurable, the isotope effect describes transition between the maximum (PT limit) and minimum (ET limit) values. The transition function can be derived from Eq. (4).

In PT variants, $k^{(2)}_{AB}$ is significantly (2–3 orders of magnitude) smaller than in native RC. The decreased rate, however, does not include necessarily that the RC variant should be a PT mutant. In ET limit, $k^{(2)}_{AB}$ decreases if the protonated fraction of Q_B^- decreases (see Eq. (1)). This can be achieved by lowering the (operational) pK_a of Q_B^-/Q_BH. Our results showed that the decrease could be substantial in different ET mutants (Fig. 4). Accordingly, the observed rate can be as low as experienced in PT mutants. In H173EQ mutant, $k^{(2)}_{AB}$ is greatly inhibited and drops to a value as low as that of the native RC treated by transition metal ion (Figs. 3a and b). Although H173EQ appears to be a borderline in terms of ET vs. PT rate limitation, it remains ET mutant [3]. The effect of mutation on the PT rate is indeterminate and could be essential. This view is supported by independent methods of ET measurements [39] and driving force assay [13,18].

The solvent isotope effect on the rate constant of the second ET exhibits features indicating that the observed kinetics are not caused by an elementary process such as the shift of pK_a values of the protonatable groups upon solvent deuteration (equilibrium isotope effect) or the unimolecular dissociation of an COO – H bond of an carboxylic group (kinetic isotope effect). Based on our experiments, we are led to conclude that the measured isotope effects in different RC variants may reflect several elementary processes.

Due to severe interruption of the protonation pathway by mutation or by divalent cations at the proton entry point, the Q_B^- semiquinone anion is protonated by any of the much slower alternative pathways controlled by a protonatable amino acid (A) in equilibrium with the aqueous bulk phase: $AH \leftrightarrow A^- + H^+$. The rate of protonation that limits the rate of the second ET $k^{(2)}_{AB}$ is $k_p = k'_{on} \cdot [H^+] + k_{off}$, where k'_{on} is the bimolecular rate constant of proton binding (values of $2–6 \cdot 10^{10}$ M^{-1} s^{-1} are commonly found for neutralization of strong bases [40]) and k_{off} is the rate constant of proton dissociation. The ratio $K_H = k_{off}/k'_{on}$ gives the proton dissociation constant. If the equilibrium partition between protonatable residue and solvent is sensitive to hydrogen isotopes, then equilibrium isotope effect is observed whose magnitude and pH-dependence can be expressed as

$$\frac{k^{(2)}_{AB}(H^+)}{k^{(2)}_{AB}(D^+)} = \frac{k'_{on}(H^+)}{k'_{on}(D^+)} \cdot \frac{\left(1 + 10^{pK_H - pH}\right)}{\left(1 + 10^{pK_D - pH}\right)} \cdot 10^{pK_D - pK_H}. \quad (5)$$

The bimolecular rate constants of H^+/D^+ binding are controlled by diffusion, intraprotein electrostatics and/or protein conformation and its sensitivity to H/D exchange should be minor [23]. According to Eq. (5), the magnitude of the solvent isotope effect is negligible ($k^{(2)}_{AB}(H^+)/k^{(2)}_{AB}(D^+) \approx 1$) at low pH ($\ll pK_H$ or pK_D) and approaches monotonously to the maximum value of $10^{(pK_D - pK)_H}$ at high pH ($\gg pK_H$ or pK_D). The transition occurs in two steps at pH ≈ pK_H and pH ≈ pK_D and above these pH values the isotope effect becomes pH-independent. Similar behavior is observed for PT agents M17DN/L210DN double mutant and metal poisoned native RC: the isotope effect is relatively small and pH-independent on the pH range between 5.5 and 9.5 (Fig. 3d). Good correspondence with the theory of equilibrium isotope effect is obtained by assumption of highly acidic residue ($pK_H \ll 5.5$) and of relatively small increase of pK_H upon deuteration ($pK_D - pK_H \approx 0.3$). The intraprotein conditions of the RC are adequate to satisfy these assumptions. The Q_B binding pocket is rich of carboxylic acid residues and the members of the acidic cluster can supply proton for the alternative pathways. The validity of the second assumption can be supported by previous experiments. The alkaline protonatable groups responsible for binding of the first proton upon $P^+Q_A^-$ formation demonstrated small increases in the p*K*a (~0.2) and a small, pH (pD)-dependent slowing of the binding rate after incubation in D_2O [23]. Although not the same groups participate in the uptake of the first and second protons, the effect of deuteration of RC on binding of the H^+/D^+ ions after the first flash can be informative on the same effect after the second flash.

Large solvent isotope effect was observed in L213DN PT mutant (Fig. 3d) that calls for a X-H(D) bond-breaking step characteristic of the kinetic isotope effect. The origin of the primary isotope effect is the difference in the frequencies of various vibrational modes of the residue, arising when H is substituted for D (Fig. 2). The large kinetic isotope effect is due to the large percentage mass change upon replacement of hydrogen with deuterium. At ambient temperature, the vibrational modes for bond stretches are dominated by the zero-point energy (ZPE). The O – H(D) bond of interest is 100% broken at the dissociation limit. In this case, the maximum possible isotope effect can be calculated from the difference of the ZPE values of the OD and OH vibrations:

$$\frac{k_H}{k_D} = \exp\left(-\frac{h\ c\ \overline{\nu_H}\left(\sqrt{\frac{\mu_{OH}}{\mu_{OD}}} - 1\right)}{2\ k_B\ T}\right) \quad (6)$$

where h is the Planck constant, c is the speed of light in vacuum, $\overline{\nu_H}$ is the wave number of O – H stretch and $\mu_{OH} = 1.06$ and $\mu_{OD} = 1.78$ are the

reduced (atomic) masses. The actual k_H/k_D ratio depends also on the ZPE values of the intermediate protonation states of the proton delivery pathway from the bulk to Q_B^-. If the transition state is very close to the dissociation limit, i.e. the O – H(D) bond breaks upon proton transfer nearly completely, then Eq. (6) would give a reasonable approximation to the upper limit of the kinetic isotope effect. Taking $\overline{\nu_H} = 3200\ cm^{-1}$ for the wave number of vibration of the O – H bonds of macromolecular association with carboxylic acid, Eq. (6) offers $k_H/k_D = 6.0$ for the maximum primary isotope effect at room temperature ($T = 293$ K).

Such a high value was obtained for the L213DN mutant in the highly acidic pH range only and in all other cases the measured isotope effects were smaller. Although the deceleration of the ET in RCs blocked with different transient divalent metal ions (Ni^{2+} and Cd^{2+}) were different (Fig. 3b), they gave similar solvent isotope effects ($k_H/k_D \approx 2.1$). This indicates that the observed isotope effects reflect changes upon deuteration in the protein rather than the mode of sealing of the proton entry point. It can occur that the PT reactions do not involve bonds that are completely broken in the transition state (the O – H bond is only partially broken) and/or another is starting to form at the transition state. Both attenuate the isotope effect from that of total homolysis used to approximate the maximum isotope effect.

To understand the pH-dependence of the isotope effects in the L213DN mutant, the ZPE of the various vibrations of the reactant and the activated complex should be compared. Primary kinetic isotope effect is observed if the ZPE difference in the activated complex/transition state is smaller than in the reactants, resulting in a difference in activation energy between O – H and O – D (Fig. 2). The magnitude of a primary kinetic isotope effect depends on differences in the ZPE's in the reactant and the activated complex for all the vibrational modes of the reactant and activated complex. In L213DN mutant, the ZPE levels of O – H and O – D vibration profile of the transition state exhibit pH-dependence in a manner of monotonous increase of the ZPE difference at higher pH. The pH-drop of the observed kinetic isotope effect can be formally approximated by a Henderson–Hasselbalch curve centered at pH 5.65 (Fig. 3d). It looks like the deprotonation of a protonatable group of $pK_a = 5.65$ would control the vibrational energy profile of the rate-determining residue in the PT. The identification of this residue and characteristics of the interaction are beyond the capacity of our work.

4.2. Changes of thermodynamics upon deuteration

Fundamental thermodynamic analysis of the second ET in PT variants can contribute to deeper understanding of the PT mechanism. The breakdown of the temperature-dependence into total enthalpy and entropy of activation has proved highly suggestive (Figs. 6 and 7), although the enthalpy and entropy contributions of the $P^* \rightarrow P^+Q_A^-$ free energy drop seriously challenged existing notions [41,42]. The wild type shows a rather small activation enthalpy that is not influenced by H/D exchange of the solvent. Any manipulations of the proton pathway by mutation or by divalent cations result in a larger net enthalpy of activation and less negative entropy. This partial offset is almost certainly not a significant "enthalpy–entropy compensation" [43,44]. The tendency remains the same upon deuteration: the enthalpy increases further and the entropy becomes less negative. The change caused by H/D exchange is small in RC inhibited by Ni^{2+} and large in L210DN/M17DN double mutant where the activation process is almost entirely enthalpic. The small entropy of activation indicates no major conformational changes of the protein upon proton delivery and accounts for slight rearrangement of the hydrogen bonded network, including solvent water, as has been well supported for carbonic anhydrase [45] and superoxide dismutase [46] and almost visualized in bacteriorhodopsin [7]. The L213DN mutant shows somewhat different behavior. The entropic contribution is larger and indicates different kinds of limitation. The L213DN is the most drastically PT limited of any known mutant and is blocked at a site nearer the Q_B quinone. Alternate PT pathway directed either to L223S or to L212 behind L213 should be activated that can include H^+/D^+ binding, per se, in the rate limiting step.

4.3. Alternate proton pathways

As the rates of PT are dramatically decreased in PT mutants compared to that in native RC, the importance of alternate proton pathways should increase [15–17]. The alternate routes do not satisfy the very strict conditions of fast proton delivery operating in native RC. The H-bond network of protonatable residues and water molecules can be less tightly coupled and can be shorter than the length of the native pathway (~20 Å). They can lead directly to O1 of Q_B via L212E/L223S or connect to the main pathway after the site of inhibition (Fig. 1). The magnitude and pH-independence of the solvent isotope effect were similar in RCs blocked by divalent cations at the proton entry point and by double mutations at L210D and M17D sites (Fig. 3d). This suggests that several (at least two) parallel alternate routes are operational in the pathway regions near the proton entry point that rescue the PT to Q_B^- in inhibited RCs. Other routes in the interior of the protein can also contribute to the PT process where other acidic residues (e.g. H173E) and water molecules become active. The cost of the rescue of proton delivery by alternate pathways is the highly reduced transfer rate.

The L213DN mutant blocks the natural proton pathway at a site closest to the quinone and demonstrates distinct behavior. In this case, the measured $k^{(2)}_{AB}$ is much (by at least 10^4 fold) less than in native RC at pH 7 (Fig. 3b). Because $k^{(2)}_{AB}$ is PT limiting, the actual rate of PT is much more strongly ($>10^7$ fold) inhibited. The enormous drop of the rate of PT and the close to maximum kinetic isotope effect with strong pH-dependence indicate very limited possibilities of alternate proton pathways. Bridging water molecules and/or L212E can replace L213D but due to loose coupling of the groups, the transfer may include H-bond breaking (or close to this limit) step.

Acknowledgements

Thanks to TÁMOP 4.2.2.A-11/1KONV-2012-0060, TÁMOP 4.2.2.B and COST Action on "Understanding Movement and Mechanism in Molecular Machines" (CM1306) programs for financial support.

References

[1] C.A. Wraight, Intraprotein proton transfer — concepts and realities from the bacterial photosynthetic reaction center, biophysical and structural aspects of bioenergetics-Chapter 12 in: M. Wikstrom (Ed.), RSC Biomolecular Science Series, Royal Society of Chemistry, Cambridge, U.K., 2005
[2] M.R. Gunner, M. Amin, X. Zhu, J. Lu, Molecular mechanisms for generating transmembrane proton gradients, Biochim. Biophys. Acta 1827 (8–9) (2013) 892–913.
[3] C.A. Wraight, Chance and design — proton transfer in water, channels and bioenergetic proteins, Biochim. Biophys. Acta 1757 (2006) 886–912.
[4] A. Chernyshev, S. Cukierman, Thermodynamic view of activation energies of proton transfer in various gramicidin A channels, Biophys. J. 82 (2002) 182–192.
[5] R. Mikulski, D. West, K.H. Sippel, B.S. Avvaru, M. Aggarwal, C. Tu, R. McKenna, D.N. Silverman, Water networks in fast proton transfer during catalysis by human carbonic anhydrase II, Biochemistry 52 (1) (2013) 125–131.
[6] B.L. de Groot, H. Grubmüller, The dynamics and energetics of water permeation and proton exclusion in aquaporins, Curr. Opin. Struct. Biol. 15 (2005) 176–183.
[7] J.K. Lányi, Crystallographic studies of the conformational changes that drive directional transmembrane ion movement in bacteriorhodopsin, Biochim. Biophys. Acta 1459 (2000) 339–345.
[8] A. Migliore, N.F. Polizzi, M.J. Therien, D.N. Beratan, Biochemistry and theory of proton-coupled electron transfer, Chem. Rev. 114 (7) (2014) 3381–3465.
[9] V.R.I. Kaila, M.I. Verkhovsky, M. Wikström, Proton-coupled electron transfer in cytochrome oxidase, Chem. Rev. 110 (12) (2010) 7062–7081.
[10] G. Renger, Mechanism of light induced water splitting in photosystem II of oxygen evolving photosynthetic organisms, Biochim. Biophys. Acta 1817 (2012) 1164–1176.
[11] P. Maróti, M. Trotta, Artificial photosynthetic systems, in: A. Griesbeck, M. Oelgemöller, F. Ghetti (Eds.), CRC Handbook of Organic Photochemistry and Photobiology, Third edition, vol.1, CRC Press, 2012, pp. 1289–1324 (Chapter 55, Third Edition).
[12] C.A. Wraight, M.R. Gunner, The acceptor quinones of purple photosynthetic bacteria — structure and spectroscopy, in: C.N. Hunter, F. Daldal, M. Thurnauer, J.T. Beatty (Eds.),

Advances in Photosynthesis and Respiration: The Purple Phototrophic Bacteria, Springer, Dordrecht, The Netherlands, 2009, pp. 379–405.
[13] M.Y. Okamura, M.L. Paddock, M.S. Graige, G. Feher, Proton and electron transfer in bacterial reaction centers, Biochim. Biophys. Acta 1458 (2000) 148–163.
[14] M.L. Paddock, G. Feher, M.Y. Okamura, Proton transfer pathways and mechanism in bacterial reaction centers, FEBS Lett. 555 (2003) 45–50.
[15] H. Cheap, S. Bernad, V. Derrien, L. Gerencsér, J. Tandori, P. de Oliveira, D.K. Hanson, P. Maróti, P. Sebban, M234Glu is a component of the proton sponge in the reaction center from photosynthetic bacteria, Biochim. Biophys. Acta 1787 (2009) 1505–1515.
[16] J. Tandori, L. Baciou, E. Alexov, P. Maróti, M. Schiffer, D.K. Hanson, P. Sebban, Revealing the involvement of extended hydrogen-bond networks in the cooperative function between distant sites in bacterial reaction centres, J. Biol. Chem. 276 (49) (2001) 45513–45515.
[17] H. Cheap, J. Tandori, V. Derrien, M. Benoit, P. de Oliveira, J. Köpke, J. Lavergne, P. Maróti, P. Sebban, Evidence for delocalized anticooperative flash induced proton bindings as revealed by mutants at M266His iron ligand in bacterial reaction centers, Biochemistry 46 (2007) 4510–4521.
[18] M.S. Graige, M.L. Paddock, J.M. Bruce, G. Feher, M.Y. Okamura, Mechanism of proton-coupled electron transfer for quinone (Q_B) reduction in reaction centers of *Rb. sphaeroides*, J. Am. Chem. Soc. 118 (1996) 9005–9016.
[19] C.R.D. Lancaster, H. Michel, The coupling of light-induced electron transfer and proton uptake as derived from crystal structures of reaction centres from *Rhodopseudomonas viridis* modified at the binding site of the secondary quinone, QB, Structure 5 (1997) 1–22.
[20] M.L. Paddock, M.E. Senft, M.S. Graige, S.H. Rongey, T. Turanchik, G. Feher, M.Y. Okamura, Characterization of second site mutations show that fast proton transfer to Q_B^- is restored in bacterial reaction centers of *Rhodobacter sphaeroides* containing the Asp-L213 → Asn lesion, Photosynth. Res. 55 (1998) 281–291.
[21] M.J. Schilstra, F. Rappaport, J.H. Nugent, C.J. Barnett, D.R. Klug, Proton/hydrogen transfer affects the S-state-dependent microsecond phases of P6801 reduction during water splitting, Biochemistry 37 (1998) 3974–3981.
[22] M.Y. Okamura, G. Feher, Isotope effect on electron transfer in reaction centers from *Rhodopseudomonas sphaeroides*, Proc. Natl. Acad. Sci. U. S. A. 83 (1986) 8152–8156.
[23] P. Maróti, C.A. Wraight, Kinetics of H^+-ion binding by the $P^+Q_A^-$ state of the bacterial photosynthetic reaction centers: rate limitation within the protein, Biophys. J. 73 (1997) 367–381.
[24] M.L. Paddock, M.S. Graige, G. Feher, M.Y. Okamura, Identification of the proton pathway in bacterial reaction centers: inhibition of proton transfer by binding of Zn^{2+} or Cd^{2+}, Proc. Natl. Acad. Sci. U. S. A. 96 (1999) 6183–6188.
[25] L. Gerencsér, P. Maróti, Retardation of proton transfer caused by binding of transition metal ion to bacterial reaction center is due to pK_a-shifts of key protonatable residues, Biochemistry 40 (2001) 1850–1860.
[26] M.L. Paddock, P. Adelroth, C. Chang, E.C. Abresch, G. Feher, M.Y. Okamura, Identification of the proton pathway in bacterial reaction centers: cooperation between Asp-M17 and Asp-L210 facilitates proton transfer to the secondary quinone (Q_B), Biochemistry 40 (2001) 6893–6902.
[27] E. Takahashi, C.A. Wraight, Small weak acids reactivate proton transfer in reaction centers from *Rhodobacter sphaeroides* mutated at AspL210 and AspM17, J. Biol. Chem. 281 (2006) 4413–4422.
[28] E. Takahashi, C.A. Wraight, A crucial role for Asp^{L213} in the proton transfer pathway to the secondary quinone of reaction centers from *Rhodobacter sphaeroides*, Biochim. Biophys. Acta 1020 (1990) 107–111.
[29] P. Maróti, C.A. Wraight, Flash-induced H^+ binding by bacterial photosynthetic reaction centers: comparison of spectrophotometric and conductimetric measurements, Biochim. Biophys. Acta 934 (1988) 314–328.
[30] R.R. Stein, A.L. Castellvi, J. Bogacz, C.A. Wraight, Herbicide-quinone competition in the acceptor complex of photosynthetic reaction centers from *Rhodopseudomonas sphaeroides*: a bacterial model for PS II-herbicide activity in plants, J. Cell. Biochem. 25 (1984) 243–259.
[31] F. Milano, L. Gerencsér, A. Agostiano, L. Nagy, M. Trotta, P. Maróti, Mechanism of quinol oxidation by ferricenium produced by light excitation in reaction centers of photosynthetic bacteria, J. Phys. Chem. B 111 (2007) 4261–4270.
[32] K. Mikkelsen, S.O. Nielsen, Acidity measurements with the glass electrode in H_2O–D_2O mixtures, J. Phys. Chem. 64 (1960) 632–637.
[33] P.K. Glasoe, F.A. Long, Use of glass electrodes to measure acidities in deuterium oxide, J. Phys. Chem. 64 (1960) 188–190.
[34] M.S. Graige, M.L. Paddock, G. Feher, M.Y. Okamura, Observation of the protonated semiquinone intermediate in isolated reaction centers from *Rb. sphaeroides*: implications for the mechanism of electron & proton transfer in proteins, Biochemistry 38 (1999) 11465–11473.
[35] C.A. Wraight, Proton and electron transfer in the acceptor quinone complex of bacterial photosynthetic reaction centers, Front. Biosci. 9 (2004) 309–327.
[36] J. Lavergne, C. Matthews, N. Ginet, Electron and proton transfer on the acceptor side of the reaction center in chromatophores of *Rhodobacter capsulatus*: evidence for direct protonation of the semiquinone state of Q_B, Biochemistry 38 (1999) 4542–4552.
[37] C.A. Wraight, P. Maróti, Temperature dependence of the 2nd electron transfer in bacterial reaction centers, Biophys. J. 86 (1) (2004) 148A (Part 2).
[38] H. Eyring, R. Lumry, J.W. Woodbury, Some applications of modern rate theory to physiological systems, Rec. Chem. Prog. 10 (1949) 100–114.
[39] E. Takahashi, C.A. Wraight, Potentiation of proton transfer function by electrostatic interactions in photosynthetic reaction centers from *Rhodobacter sphaeroides*: first results from site directed mutation of the H-subunit, Proc. Natl. Acad. Sci. U. S. A. 93 (1996) 2640–2645.
[40] M. Eigen, Proton transfer, acid-base catalysis, and enzymatic hydrolysis, Part I. Elementary processes, Angew. Chem. Int. Ed. Engl. 3 (1964) 1–72.
[41] G.J. Edens, M.R. Gunner, Q. Xu, D. Mauzerall, The enthalpy and entropy of reaction for formation of $P^+Q_A^-$ from excited reaction centers of *Rhodobacter sphaeroides*, J. Am. Chem. Soc. 122 (2000) 1479–1485.
[42] D. Mauzerall, J.M. Hou, V.A. Boichenko, Volume changes and electrostriction in the primary photoreactions of various photosynthetic systems: estimation of dielectric coefficient in bacterial reactions centers and of the observed volume changes with the Drude–Nernst equation, Photosynth. Res. 74 (2002) 173–180.
[43] K. Sharp, Entropy–enthalpy compensation: fact or artifact? Protein Sci. 10 (2001) 661–667.
[44] A. Cooper, C.M. Johnson, J.H. Lakey, M. Nöllmann, Heat does not come in different colours: entropy–enthalpy compensation, free energy windows, quantum confinement, pressure perturbation calorimetry, solvation and the multiple causes of heat capacity effects in biomolecular interactions, Biophys. Chem. 93 (2002) 215–230.
[45] J.E. Jackman, K.M. Merz, C.A. Fierke, Disruption of the active site solvent network in carbonic anhydrase II decreases the efficiency of proton transfer, Biochemistry 35 (1996) 16421–16428.
[46] W.B. Greenleaf, D.N. Silverman, Activation of the proton transfer pathway in catalysis by iron superoxide dismutase, J. Biol. Chem. 277 (2002) 49282–49286.